

REVIEW

# Practical tips and tricks in measuring strain, strain rate and twist for the left and right ventricles

Christopher Johnson MSc<sup>1,\*</sup>, Katherine Kuyt BSc<sup>2,\*</sup>, David Oxborough PhD<sup>1,†</sup> and Martin Stout PhD<sup>2,†</sup>

<sup>1</sup>Research institute for Sport and Exercise Sciences, Liverpool John Moores University, Liverpool, UK

<sup>2</sup>School of Healthcare Science, Manchester Metropolitan University, Manchester, UK

Correspondence should be addressed to D Oxborough: [d.i.oxborough@ljmu.ac.uk](mailto:d.i.oxborough@ljmu.ac.uk)

\*C Johnson and K Kuyt contributed equally as joint lead authors)

†(D Oxborough and M Stout contributed equally as joint senior authors)

## Abstract

Strain imaging provides an accessible, feasible and non-invasive technique to assess cardiac mechanics. Speckle tracking echocardiography (STE) is the primary modality with the utility for detection of subclinical ventricular dysfunction. Investigation and adoption of this technique has increased significantly in both the research and clinical environment. It is therefore important to provide information to guide the sonographer on the production of valid and reproducible data. The focus of this review is to (1) describe cardiac physiology and mechanics relevant to strain imaging, (2) discuss the concepts of strain imaging and STE and (3) provide a practical guide for the investigation and interpretation of cardiac mechanics using STE.

### Key Words

- ▶ left ventricle
- ▶ right ventricle
- ▶ strain
- ▶ strain rate
- ▶ twist
- ▶ deformation
- ▶ speckle tracking echocardiography

## Introduction

The assessment of myocardial function provides a core component of the echocardiographic examination. Traditionally this has been underpinned by the assessment of left ventricular ejection fraction (LVEF), but increasingly speckle tracking echocardiography (STE) is being used in both research and clinical environments to directly assess myocardial wall deformation (strain). This article reviews the underlying physiology, introduces the concepts of strain and provides a practical guide for acquisition, analysis and subsequent interpretation.

## Cardiac mechanics, anatomy and physiology

In order to maintain metabolic demands, cardiac architecture links closely with electrical activation and

coronary blood flow. Electrophysiological processes propagate contraction of cardiac muscle filaments via excitation–contraction coupling. However, myocytes are known to only contract by approximately 15–20% (1). To maximise efficiency, myocardial fibre arrangement and interaction becomes integral to produce adequate stroke volume for each cardiac cycle.

Each myocyte is arranged in a ‘scaffold’ that maintains the arrangement of cardiac cells and the muscle fibres in the required configuration (2). In the left ventricle (LV), the myocardium is arranged in three distinct layers. The sub-endocardium (innermost), the mid-myocardium and the sub-epicardium (outermost). The interaction of these layers plays a key role in ensuring stroke volume and hence overall cardiac output. The LV uniquely possesses a double helical myocardial fibre arrangement. That is, fibres in the sub-endocardium are arranged in a

left-handed helix, then smoothly transition to a transverse circular arrangement in the midmyocardium and then finally a right-handed helix in the epicardium (3) (Fig. 1).

During ventricular systole, there is shortening of the muscle fibres in all three layers of the LV myocardium subsequently leading to reductions in both LV length and circumference. As a result of the myocardium being an incompressible structure, there is resultant thickening of the LV myocardial walls (the thickening of the LV myocardium as seen on 2D echocardiography). This myocardial deformation can be termed longitudinal, circumferential and radial. In addition, as all three layers of fibres shorten in ventricular systole (but largely governed by the larger radius of the subepicardial fibres), there is rotation of the LV base in a clockwise direction and LV apex in an anticlockwise direction, commonly termed LV twist (Fig. 2) (4).

LV deformation largely governs the overall cardiac contraction and as such impacts significantly on the deformation of the other chambers. The interventricular septum is shared by both ventricles and septal deformation properties are largely controlled by those of the LV, but septal movement is also integral to right ventricle (RV) contraction and stroke volume (5).

The RV has a complex geometry that varies in appearance depending on the plane of imaging. The RV appears triangular when viewed from the side, yet in cross section, it appears crescent shaped (5). Physiological loading conditions result in the interventricular septum being shaped concavely towards the LV in both systole and diastole. The volume of the RV is larger than that of the LV in a normal healthy adult, but the RV walls are much thinner with overall RV mass approximately one-sixth of LV mass (6). The RV myocardium also

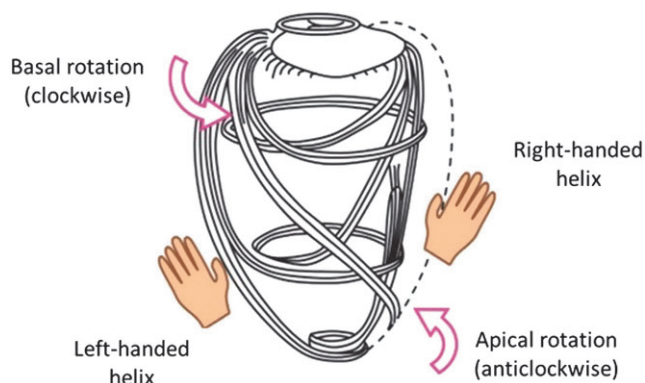


**Figure 1**  
Myocardial fibre arrangement of the sub-endo, mid and epicardium. Reproduced, with permission, from Nakatani 2011 (4).

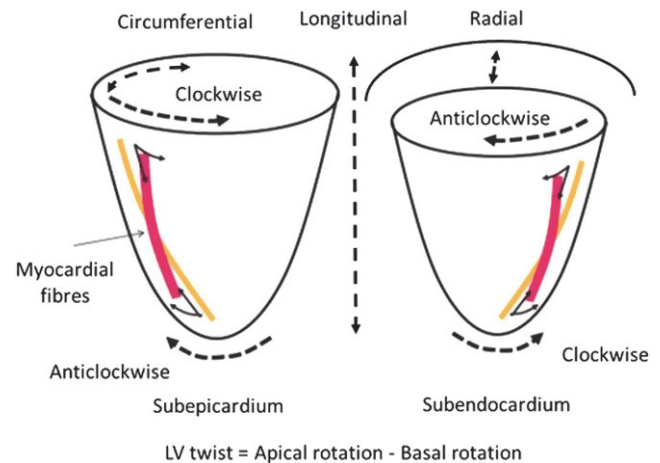


**Figure 2**  
Myocardial deformation relating to fibre architecture. Adapted, with permission, from Nakatani 2011 (4).

comprises multiple fibre layers, which can be split into the superficial and deep. The deep muscle fibres in the RV are arranged longitudinally, whereas the superficial (subepicardial) layers are arranged circumferentially, and parallel to the atrioventricular groove (7). The RV superficial fibres connect to the myofibers of the LV via the cardiac apex, thereby adding further LV influence over RV deformation (5).

The RV also deforms longitudinally, circumferentially and radially. However, the key overall deformation is shortening of the longitudinal fibres during ventricular systole (8). RV free wall radial contraction can be noted visibly during transthoracic echocardiography (TTE) but is less in magnitude than the LV because of its higher surface-to-volume ratio. Finally, there is traction of the RV-free wall at its points of LV attachment, secondary to LV deformation (5). There is no evidence of a significant layer of obliquely orientated myocardial fibres associated with the RV; therefore, there is no powerful influence of twist mechanics to overall RV contraction. Circumferential and radial RV deformation is currently not routinely measured due partially to less influence on RV function, and the limitations of commercially available technology that can accurately track the thinner walls of the RV.

## Strain measurement and STE

Strain is a measure of deformation of the myocardium during the cardiac cycle in multiple directions; lengthening, shortening and thickening. STE is a common technique used to measure strain. STE is based on grey-scale images obtained during echocardiography and has

been developed to be angle independent, a key advantage over previous methods used to derive strain. These grey-scale echocardiographic images are composed of several bright speckles resulting from the ultrasound-myocardial tissue interaction. Specialist software is able to identify the speckles and track them frame by frame during the cardiac cycle using either of two processes known as the sum of the absolute differences or Fourier analysis (Fig. 3) (9). The sum of absolute differences algorithm fits correlation-weighted data into a spatial polynomial curve in order to calculate regional strain at approximately 3 mm intervals (10). Fourier analysis assumes coherence of the geometry tracked using a sequence of intermediate passages from 2 cm down to 5 pixel bands (11). Software platforms are then able to resolve the magnitude of deformation in the directions mentioned earlier to generate strain and strain rate (SR) curves (12).

During STE, deformation is calculated using the Lagrangian method (12). Lagrangian strain is defined as deformation from an original length and calculated using the following equation:

$$\epsilon_L(t) = \frac{[L(t) - L(t_0)]}{L(t_0)}$$

where,  $L(t)$  is the length of the object at time instance  $t$  following deformation and  $L(t_0) \approx L_0$ , that is, the length of the object when not subject to external forces.  $\epsilon_1$  is Lagrangian strain.

In more simple terms, strain is expressed as a fractional length change, where shortening is a negative value and lengthening a positive value. Figure 4 shows the concept of Lagrangian strain. In order to calculate strain at any given time point, the difference between length at the reference point (end-diastole during echocardiography) and the current length (usually end-systole) is calculated.

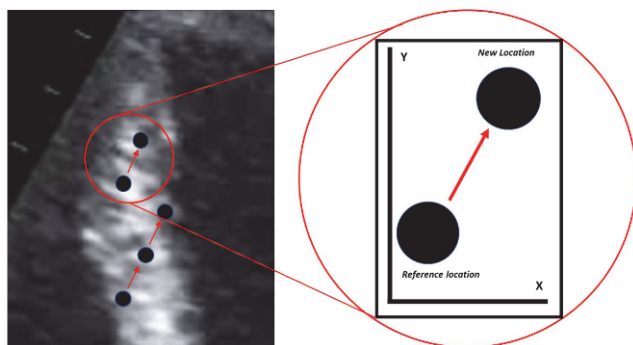


**Figure 3**  
The theoretical concept of speckle tracking echocardiography. Data from Bansal & Kasliwal 2013 (9).



**Figure 4**  
Simple diagram showing the principle of Lagrangian strain. Following deformation  $L(t)$  there is a change in length from initial reference  $L(t_0)$ . Resulting in an increased length by  $\Delta L$ . This increase in length will be expressed as a positive percentage value.

This figure is then divided by original reference length and then expressed as a percentage.

SR simply describes the rate of deformation (i.e. how quickly the deformation occurs within the cardiac cycle). SR can also be calculated using a derivative of the Lagrangian strain equation. As such, the following equation explains SR based on Lagrangian strain:

$$\epsilon_{RL}(t) = \frac{dS_L(t)}{dt} = \frac{1}{L_0} \frac{dL(t)}{dt}$$

where,  $SR_L$  is Lagrangian strain rate.  $L_0$  is the reference length at time  $t_0$  (usually end diastole). Natural strain may also be used to assess deformation and deformation rate. Natural strain uses a constantly changing reference length integrated from SR:

$$\epsilon_N(t) = \int_{t_0}^t d\epsilon_N(t)$$

However, STE is calculated using Lagrangian strain because the baseline length (end-diastole) is always known and utilised as a reference (12). Natural strain will therefore not be referred to further in this review.

It must be emphasised that as the heart is a 3D structure, there are six 'strains' placed on the myocardium. These include the three strains already mentioned (longitudinal, radial and circumferential) and in addition, three directions of 'shear' strain produced from the movement of plane layers over each other (13). When the myocardium contracts, the three layers of myocardial muscle fibres each contract, and due to the different orientation of the muscle fibres in each layer, they move over one another in a shearing motion. Shear strain plays a key role in both radial thickening and twisting of the LV, enabling systolic thickening of the myocardial wall significantly beyond the 10% thickening of each individual myocyte (14). Shear strain gradient increases as you progress from the sub-epicardium towards the

sub-endocardium and correlates with increasing radial thickening during systole.

## Optimal image acquisition

All images used for LV and RV strain analysis are acquired as part of the minimum dataset for a standard adult TTE (15). It is important however to consider the technical aspects of image acquisition that are specific to STE providing optimal images for post processing and hence maximising validity and reproducibility. It is essential to acknowledge that there are numerous software platforms that provide the functionality to post-process raw grey-scale images for STE, each with individual nuances. The following sections provide insight into these technical considerations allowing for a standardised approach but with the aim to provide theoretical underpinning irrespective of vendor differences.

### Electrocardiographic (ECG) gating

ECG gating is required for timing of events throughout the cardiac cycle and is of utmost importance in STE analysis. An optimal ECG signal with minimal heart rate (HR) variability should be present across three cardiac cycles in patients with normal sinus rhythm. The presence of significant HR variability will limit the calculation of global strain values, which is especially problematic in patients with atrial fibrillation (16). The acquisition of three cardiac cycles ensures at least one full cardiac cycle is present, and the cycle with the optimal endocardial delineation can be selected for speckle tracking.

### Frame rate

Images should be maintained at a frame rate between 40 and 90 frames per second for analysis of cardiac deformation (17). As HR increases mechanical events throughout the cardiac cycle are shortened and therefore require a higher frame rate to allow optimal STE. Therefore, investigations involving increased HR, such as exercise and pharmacological stress testing, require a proportional increase in frame rate. Lower frame rates may cause unsatisfactory STE due to reduced temporal resolution and possible speckle drop out resulting in an underestimate strain values (18). Conversely, too high a frame rate (>100 frames per second) may cause the STE algorithm to be unable to identify absolute change in the speckle pattern and inadequately track the myocardium.

This is also problematic during higher HR's and therefore it is important to maximise image quality and other settings whilst subjectively monitoring myocardial tracking.

### Image quality

STE relies on the acquisition of high-quality images. Images should be acquired using the optimal gain settings and breath-hold techniques to clearly delineate the endocardial and epicardial borders and to avoid artefact related to excess noise, rib or lung movements and translational motion of the heart (18). Furthermore, image width and depth should be focused on the chamber of interest. It is important to note that although STE is less angle dependent than TDI measures of strain, the components of longitudinal and circumferential strains are opposite in polarity to radial strain therefore any deviation from the major axis will result in a progressive reduction in strain values in the relative axis (19). In view of this, it is essential to avoid apical foreshortening in the apical views and ensure circular LV chamber in the parasternal short axis (PSAX) views whilst avoiding the use of non-standardised views (20). Suboptimal image acquisition may result in poor speckle tracking. If in a single view two or more segments are not adequately tracked, then the calculation of global strain values is restricted (21).

### Standardised views

STE analysis to produce LV global longitudinal strain (GLS), global circumferential strain (GCS), global radial strain (GRS) and rotation, twist and torsion curves relies on the acquisition of specific views (Fig. 5). Three apical views including the four chamber (A4CH), two chamber (A2CH) and long axis (APLAX) allow the analysis of GLS. GCS and GRS are processed from the PSAX view at the basal level, defined at the level of the mitral valve (MV) leaflet tips and papillary muscle (PM) level, whilst a PSAX view at the apical level, defined as the level just above the point of systolic cavity obliteration, allows the assessment of rotation/twist. RV GLS requires the acquisition of a RV focused A4CH view. This view is achieved by lateral translation of the probe from the conventional A4CH view. The optimal RV focused A4CH view should provide the maximum RV basal diameter, visualising the whole of the RV-free wall, from the tricuspid lateral annulus to the RV apex, whilst avoiding foreshortening of the RV apex, throughout the cardiac cycle (21, 22). In addition to 2D images, acquisition of spectral Doppler traces of the MV, tricuspid valve (TV), aortic valve (AV) and pulmonary

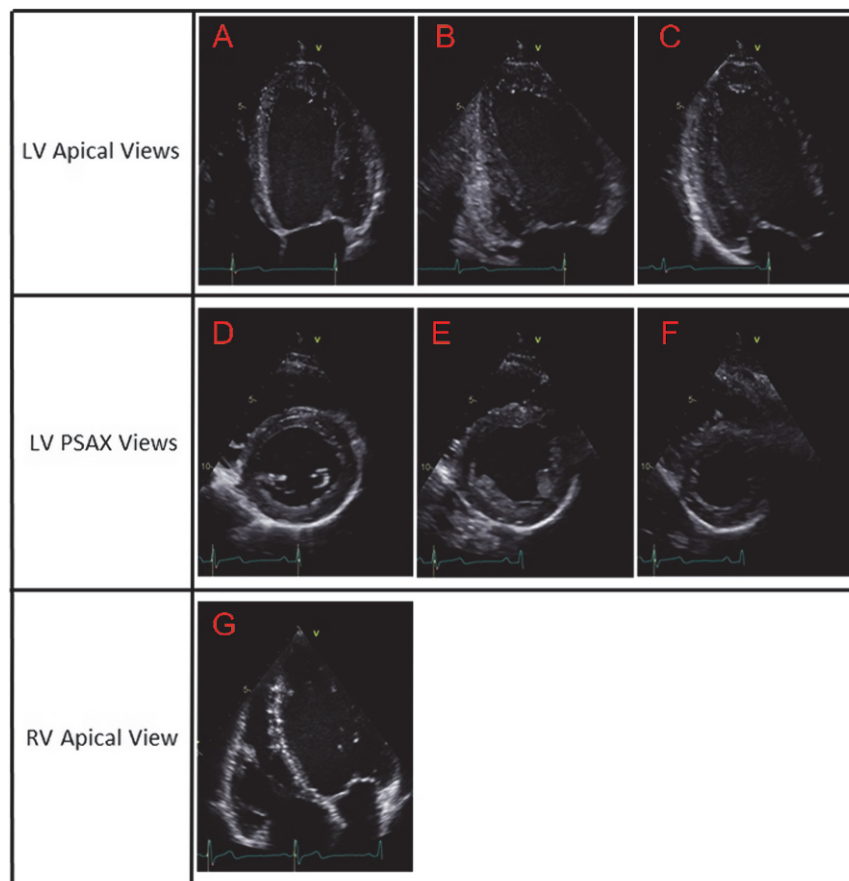


**Figure 5**

Standardised views required for speckle tracking echocardiography. Left ventricular focused apical views include (A) four-chamber, (B) two-chamber and (C) long axis. Parasternal short axis views at the level of (D) mitral valve, (E) papillary muscle and (F) apex. Right ventricular focused apical view (G) four chamber. LV, left ventricle; PSAX, parasternal short axis; RV, right ventricle.

valve (PV), allow the definition of true LV and RV end-diastolic and end-systolic event timing.

### Contrast echocardiography

The feasibility and utility of STE strain analysis in contrast TTE studies is a controversial topic. Current EACVI guidelines for contrast TTE do not refer to strain measurements, and commercially available echo machines do not allow the user to measure strain, whilst the contrast protocol is active. However, there have been some studies investigating the use and feasibility of measuring strain during a contrast-enhanced TTE. These have produced varied results. Zoppellaro *et al.* used the flash replacement technique, a form of myocardial contrast echocardiography to visualise the myocardium in 40 patients. Non-contrast and contrast images were then analysed for longitudinal strain. They found that the longitudinal strain calculated from the non-contrast and contrast-enhanced images were statistically different ( $-18.8 \pm 4.5\%$  and  $-22.8 \pm 5.4\%$ , respectively;  $P < 0.001$ ),

but their correlation was good (ICC 0.65, 95% CI 0.42–0.78) (23). Medvedofsky *et al.* reported good agreement between both contrast and non-contrast images (ICC  $r = 0.85$ ), and between contrast STE- and CMR-derived strain (ICC  $r = 0.83$ ) (24). Nagy *et al.* investigated whether deformation analysis provided additional diagnostic sensitivity beyond just wall motion scoring (WMS) during dobutamine stress echocardiography. They concluded that although STE analysis was feasible, it did not add diagnostic benefit over expert WMS alone (25). All of the above studies performed the STE analysis retrospectively using offline specialist software.

### Image analysis

Once optimal images have been acquired they should be transferred to the appropriate workstation for post processing. During post processing, it is important to replicate the analysis used in previous investigations of the same patient.

### Event timing

The accurate definition of two reference points in each region throughout the cardiac cycle is imperative for successful tracking and subsequent analysis. These reference points relate to onset and termination of myocardial contraction (end diastole and end systole, respectively). Small deviations in definition of end diastole and end systole have been reported to influence strain values significantly and at a clinically relevant magnitude (26).

End diastole is defined as the reference position/length to which systolic deformation is measured. End diastole and end systole correspond to mitral/tricuspid valve closure (MVC/TVC) and aortic/pulmonary valve closure (AVC/PVC) for the LV and RV, respectively. It is common for the software to automatically define or utilise surrogate markers of event timings, such as automated AVC detection algorithms or peak R wave detection on the ECG for MVC. This can cause deviations from true event timing in patients with conduction delays, and therefore, differences in subsequent strain values. It is therefore recommended that the sonographer visually interrogates the APLAX view frame by frame as this view

allows simultaneous visualisation of event timing (AVC and MVC) and myocardial function (26). The optimal surrogate, with the closest accuracy to 2D interrogation of MVC and AVC, is spectral Doppler of the MV and AV, respectively (26).

### Region of interest

The assessment of STE is based on subjective selection of the optimal ROI when tracking the myocardial wall (Fig. 6). Due to the complex anatomical structure of the myocardium and the distinct contribution of each myocardial layer to contraction, it is important to encompass the whole of the myocardium from the subendocardial border to the subepicardial border (13). In normal healthy individuals, the inner (subendocardial) layer contributes the most to longitudinal and circumferential strain, with a reduction in the mid-myocardium, and the lowest contribution from the outer (subepicardial) layer (27). Therefore, the width of the ROI has significant effects on the strain values reported (20, 28). If the tracking area width is too narrow, encompassing only the endocardial layer, higher strain values will be reported (28). A tracking area width larger

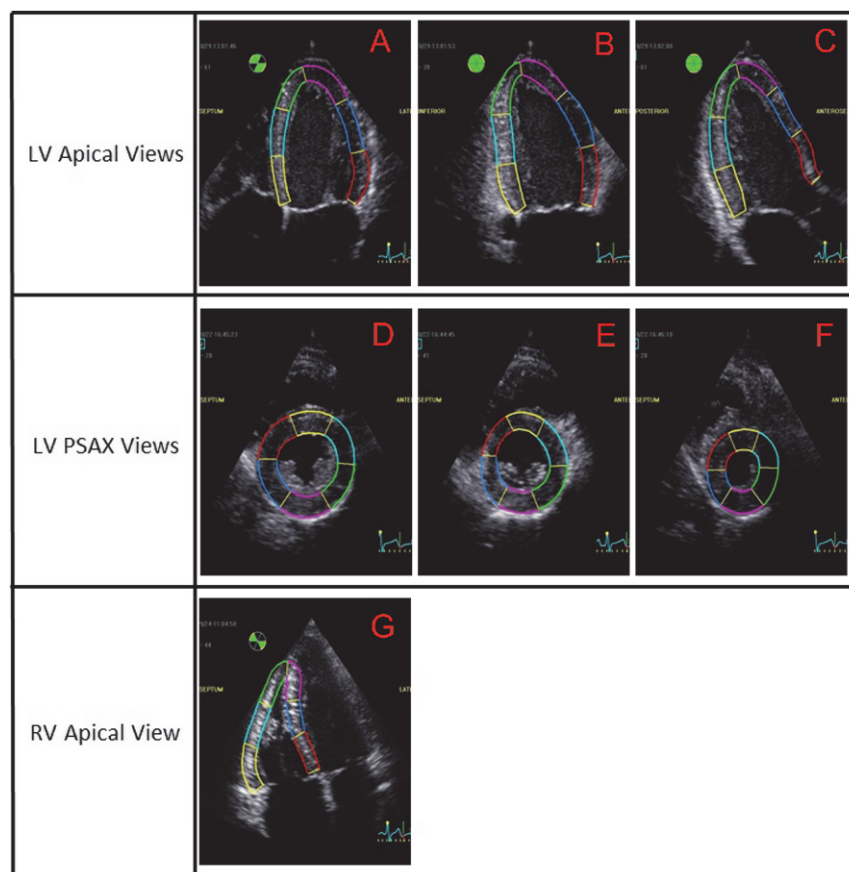


**Figure 6**  
Correct region of interest placement. Left ventricular focused apical (A) four-chamber, (B) two-chamber, (C) long axis, parasternal short axis at the levels of the (D) mitral valve, (E) papillary muscles, (F) apex and (G) right ventricular focus apical four chamber.

than the myocardium, encompassing the pericardium and excess tissue (PMs, trabeculation, etc.), can result in an underestimation of strain (28). Recommendations suggest it is important for vendors to provide accurate information pertaining to the spatial extent of the ROI (13). Further to this, care should be taken in the apical views when selecting start and end points of the ROI (Fig. 6). In the A4CH view the ROI should begin at the septal MV annulus, progress to the apex and end at the lateral MV annulus. In the APLAX view the ROI should begin at the MV annulus of the posterior wall, progress to the apex and end at the base of the septal wall taking care not to extend into the LV outflow tract. The automatically generated ROI should be visually assessed by the sonographer with manual correction of inadequate contouring recommended.

### LV longitudinal strain and SR

Longitudinal strain represents the change in length (shortening in systole, represented as a negative strain value) of the myocardium along the long axis of the LV (base to apex). Longitudinal SR represents the rate at which the deformation occurs, producing a negative value in systole and positive values in diastole. GLS is averaged from 16, 17 or 18 regional segments across three apical views (21). The segmental division at basal- and mid-level are homogeneous across the three models, with the inclusion of six segments at each level. Differences across the segmental models relate to the division of the apical level. With the 17-segment model dividing the apical level into five segments (anterior, septal, inferior and lateral, with the addition of an 'apical cap'). Alternatively the 16- and 18-segment models divide the apex into four and six equal segments, respectively. A consensus recommendation is yet to be addressed; however, local standardisation is recommended.

### LV circumferential strain and SR

Circumferential strain represents the change in length (shortening in systole, represented as a negative strain value) of the myocardium along the circumferential axis of the LV as viewed in the short axis. Circumferential SR represents the rate of circumferential deformation, with a negative systolic value and positive diastolic values. GCS is averaged from 12 regional segments across 2 PSAX views; 6 segments at MV level and 6 segments at PM level.

### LV radial strain and SR

Radial strain represents the change in wall thickness (thickening in systole, represented as a positive strain value) of the myocardium perpendicular to the long axis and directed towards the centre of the LV cavity. Radial SR represents the rate of thickening of the LV, producing a positive systolic value and negative diastolic values. GRS is averaged from the same 12 regional segments as circumferential strain using the PSAX views at MV and PM level.

### LV rotation, twist and torsion

As well as the three previously defined LV mechanics rotation of the myocardial architecture is present, expressed in degrees. Rotation occurs around the long axis of the LV, with basal rotation in a clockwise direction (negative value) and apical rotation in an anticlockwise direction (positive value), when viewed from the apex during systole. From rotation values, twist and torsion are calculated. Twist ( $^{\circ}$ ) is defined as the difference in apical and basal systolic rotation when viewed from the apex, with torsion ( $^{\circ}/\text{cm}$ ) calculated as the twist angle divided by distance between base and apex.

### RV longitudinal strain and SR

There are discrepancies present within the literature regarding the optimal ROI and subsequent segmental model to investigate longitudinal strain within the RV, with consensus yet to be achieved. These models include a full RV chamber six-segmental model (incorporating the interventricular septum into the calculation of RV global longitudinal strain; RV GLS) and a three-segmental model (encompassing only the RV free wall from lateral tricuspid annulus to RV insertion point on the LV in the calculation of RV free wall longitudinal strain; RV FWLS) (8). When comparing the tracking of the myocardium using the three-segment and six-segment model, it was reported that the latter was feasible in a larger portion of the subjects due to an increased frequency of inadequate free wall segment tracking when using the three-segmental model (8). Absolute strain values derived from the septum and free wall of the RV differ significantly, with higher (more negative) strain values produced by free wall deformation. Subsequently calculations of longitudinal strain differ, with higher RV FWLS than RV GLS (8). Although the septum contributes to the systolic function of the RV (29), it is traditionally seen as part of the LV architecture. Furthermore, regional assessment of

septal function is reported in LV regional and GLS, with the LV bullseye (BE) plot allowing easy visualisation of septal deformation. It is therefore suggested that the ROI should encompass both the RV free wall and septum, with longitudinal strain averaged from only the three free wall segments. RV FWLS is the default parameter to report (30).

## Measurement results/interpretation

### Strain and SR curves

The analysis software generates global strain, SR, rotation and twist curves (Figs 7 and 8). From these curves a variety

of clinically relevant values can be measured. Strain curves offer values of peak strain, time to peak strain and post-systolic index, with SR curves providing values of peak systolic, peak early diastolic and peak late diastolic SRs. Rotation curves provide peak systolic apical and basal rotation, twist and torsion values, with rotation rate curves representing peak twist and untwist rate.

### BE plots and coloured M-mode

BE plots of the LV provide regional values of peak strain, time to peak strain and post-systolic strain with corresponding colour-coded visual plot (Fig. 9). Conventionally the

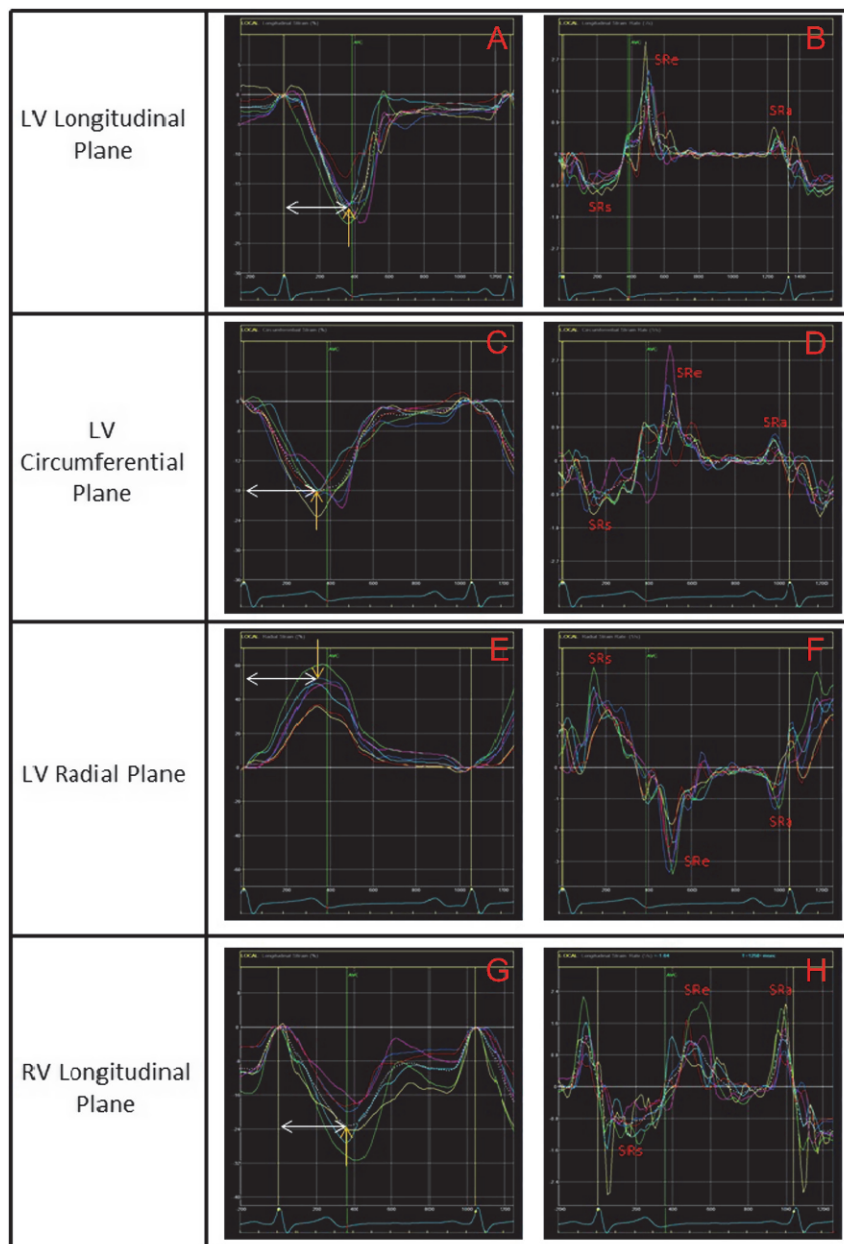


**Figure 7**

Strain and strain rate curves. (A) Left ventricular longitudinal strain and (B) strain rate. (C) Circumferential strain and (D) strain rate. (E) Radial strain and (F) strain rate. (G) Right ventricular longitudinal strain and (H) strain rate. Orange arrow indicates peak strain values. White arrow measures time to peak strain. SRs, systolic strain rate; SR<sub>e</sub>, early diastolic strain rate; SR<sub>a</sub>, late diastolic strain rate.

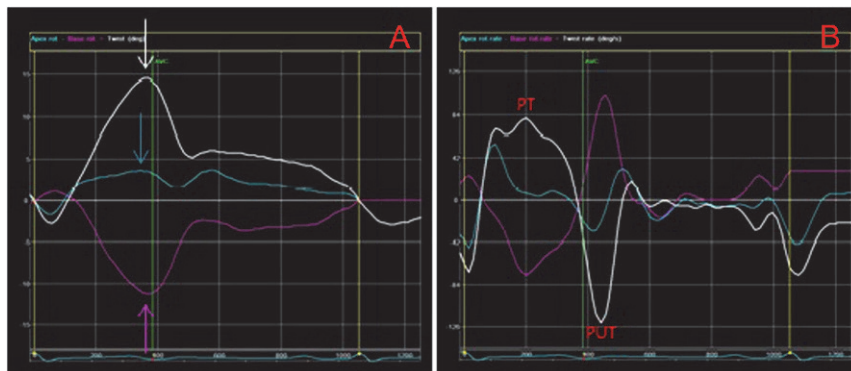


**Figure 8**

Left ventricular rotational mechanics curves. Left ventricular (A) rotation and (B) rotation rate. Blue lines represent apical rotation, pink lines represent basal rotation and white lines are twist (described previously as Twist = Apical rotation – Basal rotation). Blue arrow indicates peak apical rotation, pink arrow indicates peak basal rotation and the white arrow highlights peak twist. PT, peak twist rate; PUT, peak untwist rate.

peak strain spectrum consists of red representing normal peak strain to pink highlighting severely reduced peak strain and light blue presenting paradoxical deformation. Other colour maps to represent time to peak strain exist and highlight early time to peak strain (preceding or at AVC), late time to peak strain (proceeding AVC+250ms) and intermediate time to peak strain. The post-systolic index spectrum can be used to demonstrate deformation before AVC and delay of peak strain after AVC. The BE plot therefore allows easy visualisation of regional dysfunction and dyssynchrony. A colour m-mode map also provides colour coded grading of regional strain using the same spectrum as the BE plot.

### Normative values

The most commonly measured strain parameter in both research and clinical practice is currently longitudinal strain of the LV. Normal values for GLS have been reported in numerous studies either when comparing against pathology or when attempting to define normality in a healthy population. A comprehensive meta-analysis (31) attempted to define the normal expected ranges for GLS

in a healthy adult population. From 24 eligible studies and 28 valid datasets comprising 2597 participants, normal values for GLS varied from  $-15.9$  to  $-22.1\%$  (mean  $-19.7\%$ , CI  $-20.4$  to  $-18.9\%$ ). Meta-regression analyses showed that age, gender, body mass index, frame rate and vendor were not deemed significant sources of variation among normal ranges of GLS. Mean blood pressure was independently associated with higher values of strain.

Prospective GLS data were obtained in the EACVI NORRE study (32). NORRE was a large multi-centre European study performed within the realms of the European Association of Cardiovascular Imaging (EACVI). The study recruited 549 participants with mean age  $45.6 \pm 13.3$  years, 227 males and 322 females establishing normal ranges for GLS of  $-22.5 \pm 2.7\%$ . Similar to conventional measures of LV function, there was a significantly ( $P < 0.05$ ) higher reference value for GLS in females when compared to males ( $-23 \pm 2.7\%$  versus  $-21.7 \pm 2.5\%$ ). The absolute lowest expected values for GLS were  $-16.7\%$  in males and  $-17.8\%$  in females. Unlike the previous study (31), there was a significant decline in GLS in females between age ranges 20 and 40, 40 and 60 and  $>60$  years.

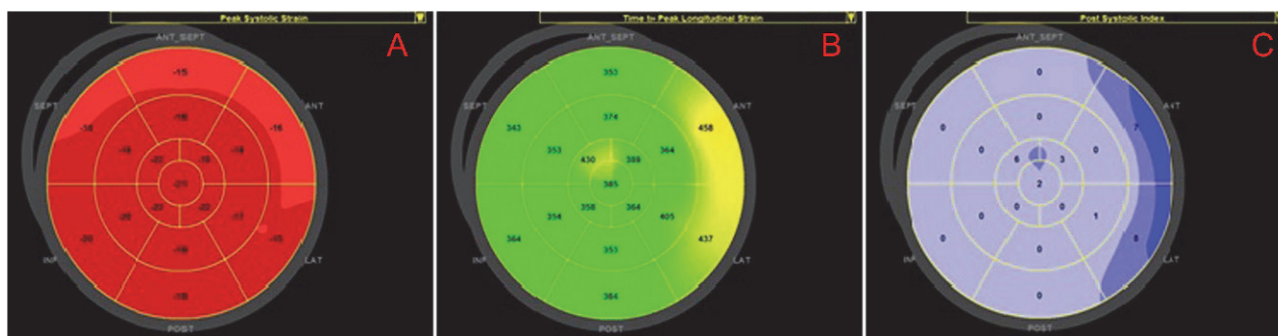


**Figure 9**

Left ventricular bullseye plots. (A) Peak systolic strain, (B) time to peak longitudinal strain and (C) post-systolic index. The outermost ring represents basal level segments, the second ring represents mid-level segments and the inner most ring represents apical level segments, with the centre circle representing the apical cap. ANT, anterior; INF, inferior; LAT, lateral; POST, posterior; SEPT, septal.

Both these studies have also attempted to classify normal circumferential and radial strain parameters for the LV. The previously referenced meta-analysis presented normal GCS reference values from  $-20.9$  to  $-27.8\%$  (mean  $-23.3\%$ , 95% CI  $-24.6$  to  $-22.1\%$ ). These data were obtained from 14 independent studies consisting of a total of 599 patients. GRS values ranged from 35.1 to 59% (mean 47.3%, 95% CI 43.6–51%), from 568 patients from 12 studies. NORRE (32) measured GCS and GRS in their 549 participants. Average GCS was  $-31.9 \pm 4.5\%$  and average GRS  $37.4 \pm 8.4\%$ . Again, there was higher GCS and GRS in females when compared to males (difference in GCS non-significant). Lowest expected values for GCS were  $-22.3\%$  for males and  $-23.6\%$  in females, whilst the lowest cut-off values for GRS were 20.6% for males and 21.5% for females.

The reproducibility of strain is variable with suggested inter-vendor variability in the measurement of GLS (33). Inter- and intra-observer reproducibility of GLS (33) and GCS (34) has been reported to be very good, with radial strain proving less so (34). Therefore, it is recommended that serial measurements are taken using the same machine to acquire the images and software to analyse. Where this is not possible, the other alternative is to use vendor-independent analysis software to analyse the images. This is supported by NORRE who suggest lower radial and higher values of circumferential strain will be obtained using GE equipment when compared to Phillips. There were no significant differences seen between vendors in GLS (32).

Normal values for SR using STE are less well studied and therefore there is no clear clinical consensus for these values. Normal resting values of between 1.0/s and 1.4/s (SD 0.5–0.6/s) have been suggested by leading experts for longitudinal deformation (35).

Normal values for LV rotation and twist show some variation in the literature and are dependent on the technique used for measurement, the location of the region of interest (e.g. sub-endocardium or sub-epicardium, participant age and loading haemodynamics of the LV (17)). Early studies using 118 healthy volunteers (36) have reported mean peak LV twist values of  $7.7 \pm 3.5^\circ$ . This study also noted that peak LV twist was significantly higher in participants  $>60$  years ( $10.8 \pm 4.9^\circ$ ) compared to those aged  $<40$  years ( $6.7 \pm 2.9^\circ$ ) and those aged 40–60 years ( $8.0 \pm 3.0^\circ$ ). NORRE (32) were able to collect LV twist data within their population in order to establish the reference ranges based on age and gender. Total average mean twist was  $7.9 \pm 3.1^\circ$  over the entire population. There was, however, a significant difference

in mean twist between males and females with females showing higher values ( $7.4 \pm 2.6^\circ$  males and  $8.3 \pm 3.3^\circ$  for females). The lowest expected values were  $2.2^\circ$  for males and  $1.9^\circ$  for females. There was no significant change in LV twist with increasing age.

There is conflicting agreement regarding the best method to measure RV longitudinal strain, in that the normative data are somewhat variable. A prospective study collected RV longitudinal strain data in 116 participants. Mean participant age was  $48 \pm 16$  years and 58% of the cohort was female. Participants were found to have a mean value for RV FWLS of  $-26 \pm 4\%$  (37). These data were supported by a meta-analysis conducted by the same team using ten studies and a total of 486 patients meeting strict inclusion criteria. For these studies, the mean age ranged from 43 to 57 years and 59% of the cohort was female. Normal values for STE measured RV FWLS of  $-27.2\%$  (95% CI  $-29$  to  $-24\%$ ) were suggested. RV GLS produced a normal value of  $-20.1$  (95% CI  $-20$  to  $-19\%$ ) (37). In a further prospective study conducted by leading European experts, 276 healthy participants were recruited aged between 18 and 76 years and 55% female (8). This study attempted to define the feasibility of 3-segment model (RV FWLS) and the 6-segment model (RV GLS) of RV longitudinal strain together with definition of reference ranges for both techniques. RV GLS analysis was feasible in 92% of the population. RV FWLS demonstrated higher magnitude than RV GLS. Males demonstrated lower RV longitudinal strain values independent of the 3- or 6-segment model. Reference limits of normality of  $-20\%$  for males and  $-20.3\%$  for females were suggested for RV GLS, with limits of  $-22.5\%$  for males and  $-23.3\%$  for females suggested for RV FWLS.

It is important to note the limitations of 2D STE. Firstly, as previously mentioned, the chambers of the heart are 3D structures that have sophisticated mechanics produced by complex myofiber orientation in several directions. 2D STE does not allow tracking of 'out-of-plane' speckle motion. Due to this 2D STE requires the acquisition of multiple images from several views. This gives rise to potential variation in plane slices and HR. 3D STE has the potential to eradicate these inherent limitations using a single apical view for image acquisition and allowing tracking of speckles across planes in multiple directions during post processing. 3D STE is not without its own limitations. 3D STE requires adequate temporal resolution with the suggested optimal frame rate of 35–50 FPS (38). Acquisition of a 3D data set with adequate frame rates requires compliance of the patient in multi-beat breath-hold techniques. If breath-hold and therefore multi-beat

imaging is not appropriate, 3D data sets acquired over less beats with frame rates below 18 FPS are reported to underestimate strain values (39).

## Conclusion

STE provides an accessible, feasible and reproducible investigation for cardiac deformation and rotational mechanics. Efforts towards standardisation of STE image acquisition, post processing and interpretation should be a priority in order to achieve inter-vendor, inter-software and inter-organisational compliance. This coupled with increased ease of use and rapid analysis through technological development provides an opportunity for an effective and efficient routine clinical investigation. Future implementation of STE in clinical practice could offer a further non-invasive method of investigation into cardiac function within subclinical disease populations, allowing a window of opportunity to alter patient therapy/management before pronounced dysfunction.

### Declaration of interest

The authors declare that there is no conflict of interest that could be perceived as prejudicing the impartiality of this review.

### Funding

This work did not receive any specific grant from any funding agency in the public, commercial or not-for-profit sector.

### Author contribution statement

C Johnson and K Kuyt: Joint lead authors. D Oxborough and M Stout: Joint senior authors.

## References

- Spotnitz HM. Macro design, structure, and mechanics of the left ventricle. *Journal of Thoracic and Cardiovascular Surgery* 2000 **119** 1053–1077. ([https://doi.org/10.1016/S0022-5223\(00\)70106-1](https://doi.org/10.1016/S0022-5223(00)70106-1))
- Buckberg G, Hoffman JIE, Mahajan A, Saleh S & Coghlan C. Cardiac mechanics revisited. *Circulation* 2008 **118** 2571–2587. (<https://doi.org/10.1161/CIRCULATIONAHA.107.754424>)
- Zhukov L & Barr AH. Heart-muscle fiber reconstruction from diffusion tensor MRI. *IEEE Visualization, 2003. VIS 2003*, 597–602. (<https://doi.org/10.1109/VISUAL.2003.1250425>)
- Nakatani S. Left ventricular rotation and twist: why should we learn? *Journal of Cardiovascular Ultrasound* 2011 **19** 1–6. (<https://doi.org/10.4250/jcu.2011.19.1.1>)
- Haddad F, Hunt SA, Rosenthal DN & Murphy DJ. Right ventricular function in cardiovascular disease, Part I: anatomy, physiology, aging, and functional assessment of the right ventricle. *Circulation* 2008 **117** 1436–1448. (<https://doi.org/10.1161/CIRCULATIONAHA.107.653576>)
- Lorenz CH, Walker ES, Morgan VL, Klein SS & Graham TP Jr. Normal human right and left ventricular mass, systolic function, and gender differences by cine magnetic resonance imaging. *Journal of Cardiovascular Magnetic Resonance* 1999 **1** 7–21. (<https://doi.org/10.3109/10976649909080829>)
- Ho SY & Nihoyannopoulos P. Anatomy, echocardiography, and normal right ventricular dimensions. *Heart* 2006 **92** i2–i13. (<https://doi.org/10.1136/hrt.2005.077875>)
- Muraru D, Onciul S, Peluso D, Soriani N, Cucchini U, Aruta P, Romeo G, Cavalli G, Illiceto S & Badano LP. Sex- and method-specific reference values for right ventricular strain by 2-dimensional speckle-tracking echocardiography. *Circulation: Cardiovascular Imaging* 2016 **9** e003866. (<https://doi.org/10.1161/CIRCIMAGING.115.003866>)
- Bansal M & Kasliwal RR. How do I do it? Speckle-tracking echocardiography. *Indian Heart Journal* 2013 **65** 117–123. (<https://doi.org/10.1016/j.ihj.2012.12.004>)
- Reisner SA, Lysyansky P, Agmon Y, Mutlak D, Lessick J & Friedman Z. Global longitudinal strain: a novel index of left ventricular systolic function. *Journal of the American Society of Echocardiography* 2004 **17** 630–633. (<https://doi.org/10.1016/j.echo.2004.02.011>)
- Nesbitt GC, Mankad S & Oh JK. Strain imaging in echocardiography: methods and clinical applications. *International Journal of Cardiovascular Imaging* 2009 **25** 9–22. (<https://doi.org/10.1007/s10554-008-9414-1>)
- Hoit BD. Strain and strain rate echocardiography and coronary artery disease. *Circulation: Cardiovascular Imaging* 2011 **4** 179–190. (<https://doi.org/10.1161/CIRCIMAGING.110.959817>)
- Voigt JU, Pedrizzetti G, Lysyansky P, Marwick TH, Houle H, Baumann R, Pedri S, Ito Y, Abe Y, Metz S, *et al.* Definitions for a common standard for 2D speckle tracking echocardiography: consensus document of the EACVI/ASE/Industry Task Force to standardize deformation imaging. *European Heart Journal: Cardiovascular Imaging* 2015 **16** 1–11. (<https://doi.org/10.1093/ehjci/jeu184>)
- Yuan LJ, Takenaka K, Uno K, Ebihara A, Sasaki K, Komuro T, Sonoda M & Nagai R. Normal and shear strains of the left ventricle in healthy human subjects measured by two-dimensional speckle tracking echocardiography. *Cardiovascular Ultrasound* 2014 **12** 7. (<https://doi.org/10.1186/1476-7120-12-7>)
- Wharton G, Steeds R, Allen J, Phillips H, Jones R, Kanagala P, Lloyd G, Masani N, Mathew T, Oxborough D, *et al.* A minimum dataset for a standard adult transthoracic echocardiogram: a guideline protocol from the British Society of Echocardiography. *Echo Research and Practice* 2015 **2** G9–G24. (<https://doi.org/10.1530/ERP-14-0079>)
- Kusunose K, Yamada H, Nishio S, Tomita N, Hotchi J, Bando M, Niki T, Yamaguchi K, Taketani Y, Iwase T, *et al.* Index-beat assessment of left ventricular systolic and diastolic function during atrial fibrillation using myocardial strain and strain rate. *Journal of the American Society of Echocardiography* 2012 **25** 953–959. (<https://doi.org/10.1016/j.echo.2012.06.009>)
- Mor-Avi V, Lang RM, Badano LP, Belohlavek M, Cardim NM, Derumeaux G, Galderisi M, Marwick T, Nagueh SF, Sengupta PP, *et al.* Current and evolving echocardiographic techniques for the quantitative evaluation of cardiac mechanics: ASE/EAE consensus statement on methodology and indications endorsed by the Japanese Society of Echocardiography. *Journal of the American Society of Echocardiography* 2011 **24** 277–313. (<https://doi.org/10.1016/j.echo.2011.01.015>)
- Rösner A, Barbosa D, Aarsæther E, Kjønsås D, Schirmer H & D'hooge J. The influence of frame rate on two-dimensional speckle-tracking strain measurements: a study on silico-simulated models and images recorded in patients. *European Heart Journal: Cardiovascular Imaging* 2015 **16** 1137–1147. (<https://doi.org/10.1093/ehjci/jev058>)

- 19 Forsha D, Risum N, Rajagopal S, Dolgner S, Hornik C, Barnhart H, Kisslo J & Barker P. The influence of angle of insonation and target depth on speckle-tracking strain. *Journal of the American Society of Echocardiography* 2015 **28** 580–586. (<https://doi.org/10.1016/j.echo.2014.12.015>)
- 20 Stoebe S, Tarr A, Pfeiffer D & Hagendorff A. The impact of the width of the tracking area on speckle tracking parameters – methodological aspects of deformation imaging. *Echocardiography* 2014 **31** 586–596. (<https://doi.org/10.1111/echo.12440>)
- 21 Lang RM, Badano LP, Mor-Avi V, Afilalo J, Armstrong A, Ernande L, Flachskampf FA, Foster E, Goldstein SA, Kuznetsova T, *et al.* Recommendations for cardiac chamber quantification by echocardiography in adults: an update from the American Society of Echocardiography and the European Association of Cardiovascular Imaging. *European Heart Journal: Cardiovascular Imaging* 2015 **16** 233–270. (<https://doi.org/10.1093/ehjci/jev014>)
- 22 Rudski LG, Lai WW, Afilalo J, Hua L, Handschumacher MD, Chandrasekaran K, Solomon SD, Louie EK & Schiller NB. Guidelines for the echocardiographic assessment of the right heart in adults: a report from the American Society of Echocardiography endorsed by the European Association of Echocardiography, a registered branch of the European Society of Cardiology, and the Canadian Society of Echocardiography. *Journal of the American Society of Echocardiography* 2010 **23** 685–713; quiz 786. (<https://doi.org/10.1016/j.echo.2010.05.010>)
- 23 Zoppellaro G, Venneri L, Khatter RS, Li W & Senior R. Simultaneous assessment of myocardial perfusion, wall motion, and deformation during myocardial contrast echocardiography: a feasibility study. *Echocardiography* 2016 **33** 889–895. (<https://doi.org/10.1111/echo.13190>)
- 24 Medvedofsky D, Lang RM, Kruse E, Guile B, Weinert L, Cizek B, Jacobson Z, Negron J, Volpato V, Prado A, *et al.* Feasibility of left ventricular global longitudinal strain measurements from contrast-enhanced echocardiographic images. *Journal of the American Society of Echocardiography* 2018 **31** 297–303. (<https://doi.org/10.1016/j.echo.2017.10.005>)
- 25 Nagy AI, Sahlén A, Manouras A, Henareh L, Da Silva C, Günyeli E, Apor AA, Merkely B & Winter R. Combination of contrast-enhanced wall motion analysis and myocardial deformation imaging during dobutamine stress echocardiography. *European Heart Journal: Cardiovascular Imaging* 2015 **16** 88–95. (<https://doi.org/10.1093/ehjci/jeu171>)
- 26 Mada RO, Lysiansky P, Daraban AM, Duchenne J & Voigt JU. How to define end-diastole and end-systole?: impact of timing on strain measurements. *JACC: Cardiovascular Imaging* 2015 **8** 148–157. (<https://doi.org/10.1016/j.jcmg.2014.10.010>)
- 27 Leitman M, Lysiansky M, Lysiansky P, Friedman Z, Tyomkin V, Fuchs T, Adam D, Krakover R & Vered Z. Circumferential and longitudinal strain in 3 myocardial layers in normal subjects and in patients with regional left ventricular dysfunction. *Journal of the American Society of Echocardiography* 2010 **23** 64–70. (<https://doi.org/10.1016/j.echo.2009.10.004>)
- 28 Spriestersbach H, Oh-Ici D, Schmitt B, Berger F & Schmitz L. The influence of the region of interest width on two-dimensional speckle tracking-based measurements of strain and strain rate. *Echocardiography* 2015 **32** 89–95. (<https://doi.org/10.1111/echo.12589>)
- 29 Buckberg G & Hoffman JL. Right ventricular architecture responsible for mechanical performance: unifying role of ventricular septum. *Journal of Thoracic and Cardiovascular Surgery* 2014 **148** 3166.e1–3171.e1. (<https://doi.org/10.1016/j.jtcvs.2014.05.044>)
- 30 Badano LP, Koliás TJ, Muraru D, Abraham TP, Aurigemma G, Edvardsen T, D'Hooge J, Donal E, Fraser AG, Marwick T, *et al.* Standardization of left atrial, right ventricular, and right atrial deformation imaging using two-dimensional speckle tracking echocardiography: a consensus document of the EACVI/ASE/Industry Task Force to standardize deformation imaging. *European Heart Journal: Cardiovascular Imaging* 2018 **19** 591–600. (<https://doi.org/10.1093/ehjci/jev042>)
- 31 Yingchoncharoen T, Agarwal S, Popović ZB & Marwick TH. Normal ranges of left ventricular strain: a meta-analysis. *Journal of the American Society of Echocardiography* 2013 **26** 185–191. (<https://doi.org/10.1016/j.echo.2012.10.008>)
- 32 Sugimoto T, Dulgheru R, Bernard A, Ilardi F, Contu L, Addetia K, Caballero L, Akhaladze N, Athanassopoulos GD, Barone D, *et al.* Echocardiographic reference ranges for normal left ventricular 2D strain: results from the EACVI NORRE study. *European Heart Journal: Cardiovascular Imaging* 2017 **18** 833–840. (<https://doi.org/10.1093/ehjci/jex140>)
- 33 Nagata Y, Takeuchi M, Mizukoshi K, Wu VC, Lin FC, Negishi K, Nakatani S & Otsuji Y. Intervendor variability of two-dimensional strain using vendor-specific and vendor-independent software. *Journal of the American Society of Echocardiography* 2015 **28** 630–641. (<https://doi.org/10.1016/j.echo.2015.01.021>)
- 34 Oxborough D, George K & Birch KM. Intraobserver reliability of two-dimensional ultrasound derived strain imaging in the assessment of the left ventricle, right ventricle, and left atrium of healthy human hearts. *Echocardiography* 2012 **29** 793–802. (<https://doi.org/10.1111/j.1540-8175.2012.01698.x>)
- 35 Marwick TH. Measurement of strain and strain rate by echocardiography: ready for prime time? *Journal of the American College of Cardiology* 2006 **47** 1313–1327. (<https://doi.org/10.1016/j.jacc.2005.11.063>)
- 36 Takeuchi M, Nakai H, Kokumai M, Nishikage T, Otani S & Lang RM. Age-related changes in left ventricular twist assessed by two-dimensional speckle-tracking imaging. *Journal of the American Society of Echocardiography* 2006 **19** 1077–1084. (<https://doi.org/10.1016/j.echo.2006.04.011>)
- 37 Fine NM, Chen L, Bastiansen PM, Frantz RP, Pellikka PA, Oh JK & Kane GC. Reference values for right ventricular strain in patients without cardiopulmonary disease: a prospective evaluation and meta-analysis. *Echocardiography* 2015 **32** 787–796. (<https://doi.org/10.1111/echo.12806>)
- 38 Negishi K, Negishi T, Agler DA, Plana JC & Marwick TH. Role of temporal resolution in selection of appropriate strain technique for evaluation of subclinical myocardial dysfunction. *Echocardiography* 2012 **29** 334–339. (<https://doi.org/10.1111/j.1540-8175.2011.01586.x>)
- 39 Yodwut C, Weinert L, Klas B, Lang RM & Mor-Avi V. Effects of frame rate on three-dimensional speckle-tracking-based measurements of myocardial deformation. *Journal of the American Society of Echocardiography* 2012 **25** 978–985. (<https://doi.org/10.1016/j.echo.2012.06.001>)

Received in final form 3 June 2019

Accepted 13 June 2019

Accepted Manuscript published online 13 June 2019